iScience

CellPress

Article

Rare Earth Doped Optical Fibers with Multi-section Core

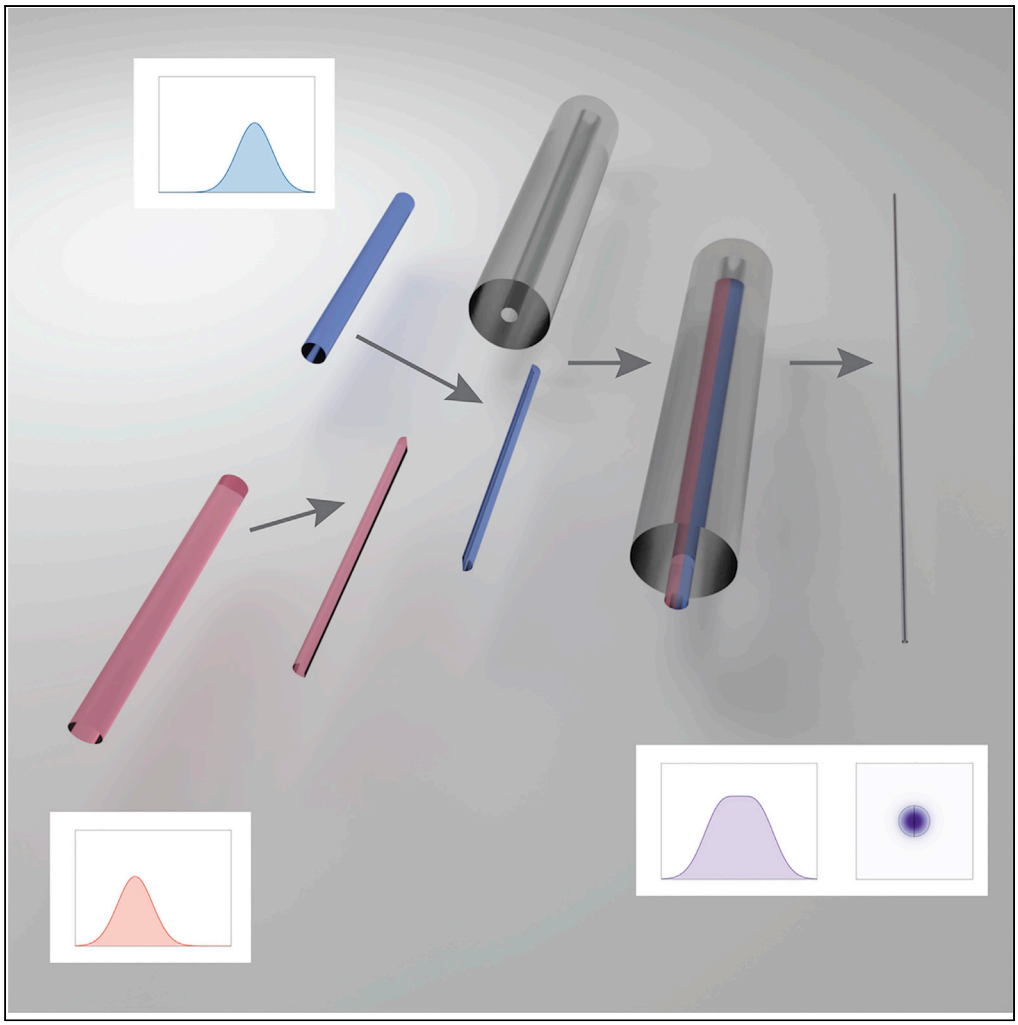

Chongyuan Huang, Jihong Geng, Tao Luo, ..., Rongguang Liang, Shanhui Fan, Shibin Jiang

sjiang@advaluephotonics.com

HIGHLIGHTS

A theoretical study of the fiber with asymmetric gain profile is presented

A multi-section core fiber is demonstrated with unique manufacturing strategy

This fiber greatly extends gain bandwidth while maintaining a good beam quality

Huang et al., iScience *22*, 423–429
December 20, 2019
https://doi.org/10.1016/j.isci.2019.11.017

iScience

CellPress

Article

Rare Earth Doped Optical Fibers with Multi-section Core

Chongyuan Huang,[1,2] Jihong Geng,[1] Tao Luo,[1] Jiali Han,[3] Qing Wang,[1] Rongguang Liang,[2] Shanhui Fan,[4] and Shibin Jiang[1,5,*]

SUMMARY

The gain bandwidth of a single-mode fiber is limited by the atomic transitions of one rare earth gain element. Here we overcome this long-standing challenge by designing a new single-mode fiber with multi-section core, where each section is doped with different gain element. We theoretically propose and experimentally demonstrate that this configuration provides a gain bandwidth well beyond the capability of conventional design, whereas the inclusion of multiple sections does not compromise single-mode operation or the quality of the transverse modal profile. This new fiber will be beneficial in realizing all fiber laser systems with few-cycle pulse duration or octave tunability.

INTRODUCTION

The invention and development of rare earth doped optical fibers led to a revolution in the design of robust and compact light sources with excellent beam quality and high conversion efficiency (Agrawal, 2007). These fiber-based sources have become essential parts in a wide range of applications, including telecommunications, nonlinear microscopy, optical coherent tomography, and material processing (Richardson, 2010; Jackson, 2012; Geng and Jiang, 2014). As the demand for better performances continually grows, fiber light sources with shorter pulse duration, wider spectrum spanning, and larger tunable range are increasingly desirable. To achieve such sources, active fibers with broader gain bandwidth are critical (Digonnet, 2001). By optimizing active ion concentration, adding co-doping ions, or adjusting host glass compositions, the emission wavelength span can be increased to some degree. However, the allowable atomic transitions of rare earth dopants impose a physical limit on the maximum gain bandwidth that can be reached (Koechner, 2006).

In fact, a gain medium with broad emission band is not only a goal being pursued by the fiber community for a long time but also a subject of great interest in semiconductors. By stacking active nanomaterials with different emission wavelengths together, several groups have demonstrated spectrally broadband light sources (Gmachl et al., 2002; Rösch et al., 2015; Fan et al., 2015). In contrast to the development in semiconductor materials, to date, the core of single-mode fiber has been limited to only one kind of gain material and thus limited bandwidth. Some previous efforts combine multiple cores in one fiber to obtain multi-color emission (Bookey et al., 2007), but such designs can only generate discrete waveband from each core and are incompatible with the fibers that are routinely used. In another approach, a mixture of different granulated rare earth oxides is melted together and forms a single core (Di Labio et al., 2008). From laser media point of view, this core is actually made of one material, in which the rare earth ions have strong interactions with each other. As a result, undesirable energy transfers occur and quench certain radiative transitions, limiting laser emission wavelengths. To isolate each dopant from other active ions and local environment, nanoparticle-based approaches have been developed and explored (Kucera et al., 2009). The nanoparticles can establish shields outside the rare earth dopants and provide the physical separation, thereby reducing the ion interaction. Although this approach seems promising compared with previous ones, it is very difficult to control the morphology of rare earth nanoparticles and maintain their integrity in the multiple thermal steps of fiber fabrication, especially when two or more different dopants are present. Therefore, it remains a significant challenge to greatly extend the gain bandwidth of a single-mode gain fiber. Alternatively, researchers have to design complex optical cavities to alleviate the material constraint (Krauss et al., 2010; Chong et al., 2012), with increasing volume and cost of the overall system.

In this article, we present a new class of single-mode fibers with gain bandwidth well beyond the limit of a single laser material. Our fibers comprise multi-section core, with each section made of a different gain

[1]AdValue Photonics Inc., Tucson, AZ 85706, USA

[2]College of Optical Sciences, University of Arizona, Tucson, AZ 85721, USA

[3]Department of Systems and Industrial Engineering, University of Arizona, Tucson, AZ 85721, USA

[4]Department of Electrical Engineering, Ginzton Laboratory, Stanford University, Stanford, CA 94305, USA

[5]Lead Contact

*Correspondence: sjiang@advaluephotonics.com

https://doi.org/10.1016/j.isci.2019.11.017

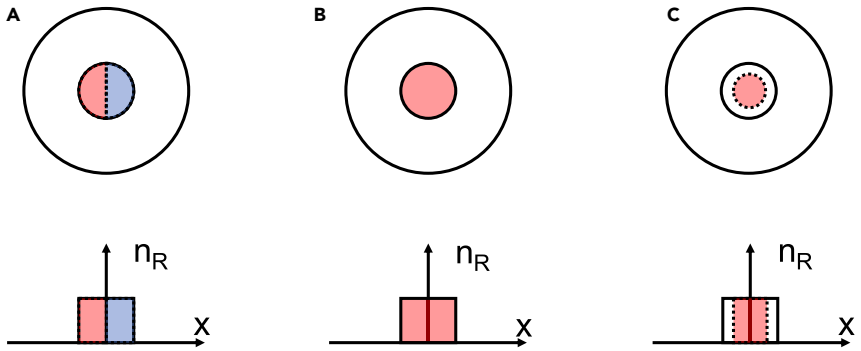

Figure 1. Comparison of Active Fiber Configurations

(A) The fiber with asymmetric gain.

(B) Conventional fibers with uniform gain filling their core.

(C) Conventional fibers with reduced gain area.

material (Figure 1A). There are two main challenges that have prevented the consideration and demonstration of this class of fibers previously. First, it is essential for fiber systems to maintain single-mode operation and the quality of the modal profile. Thus, all existing rare-earth-doped fibers have a cylindrical symmetric structure. An optical fiber typically comprises a central core surrounded by a cladding with lower refractive index. When doped with rare earth elements, the fiber is given optical gain that enables light amplification. The vast majority of rare-earth-doped fibers employ a uniform gain area overlapping with the circular core completely (Figure 1B). In some cases, the doping area is reduced smaller than the core (Figure 1C). Although the gain is no longer homogeneous in the core, it still follows a circular symmetric distribution to avoid mode distortion. Despite the large amount of research on optical fibers, so far little attention has been paid to the fibers with asymmetric gain profiles. It is not clear, without symmetric gain, whether a fiber such as shown in Figure 1A can still achieve good mode quality. Second, there are also intrinsic difficulties in experimentally achieving asymmetric structures with conventional modified chemical vapor deposition (MCVD) method, because the vapor mixtures are passed through and deposited on an axially rotated silica glass tube in the MCVD process (Li, 1985). In addition, it is not easy to precisely control and match the indices of the resultant glasses due to the limited controllability of the metal halide vapor stream.

Our work addresses the two main challenges as outlined above. Theoretically, we conducted systematic analysis to understand the mode behavior with the presence of asymmetric gain profiles, complementing current fiber mode theory (Snyder and Love, 1983; Siegman, 2003, 2007) and extending it to the complex space. Experimentally, the manufacture challenge was overcome through the rod-in-tube technique (Geng et al., 2014). Instead of conventional silica-based glasses, we demonstrated the fiber with multi-component silicate glasses, which allow us to precisely control the doping concentrations and refractive indices over a wider range than that can be achieved in silica glasses. The results show that, by weakly breaking the symmetry of the gain profile, a new degree of freedom is created and enables fibers with unprecedented performance.

RESULTS AND DISCUSSION

We first explore mode properties of optical fibers having asymmetric gain. Figure 1A depicts a fiber that, like conventional fibers, has a round core surrounded by a cladding, but its core is divided into two sections. For simplicity, we assume that only one of the regions has gain. When a light wave propagates in the core region, it will see a complex refractive index distribution $n = n_0 + n_R + in_I$, where n_0 represents a constant background index and n_R is the real index profile of the structure. The gain component n_I has a uniform value $n_{I,1} = g$ for the doped region, whereas the other section is $n_{I,2} = 0$. Then the light field $A(\vec{r}) = \phi(x, y, z)e^{-ikz}$ in a fiber can be described by the equation

$$\nabla^2 A(\vec{r}) + k_0^2 n^2(\vec{r}) A(\vec{r}) = 0 \qquad \text{(Equation 1)}$$

where $k = k_0 n_0$ with $k_0 = 2\pi/\lambda$ and λ the wavelength of light in vacuum. Substitution of A into the equation and making the paraxial approximation yield

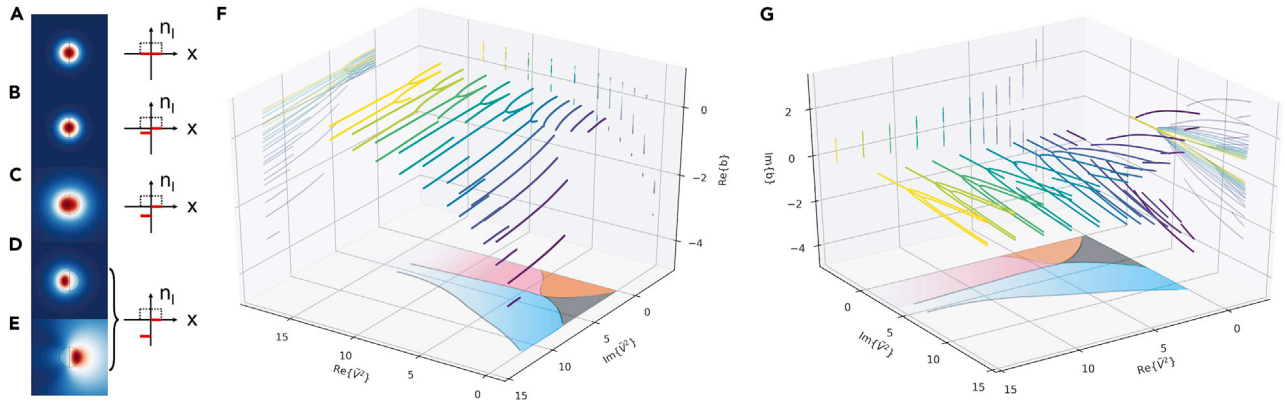

Figure 2. The Fiber Modes with Asymmetric Gain

(A–E) Typical behavior of modal field when gain coefficient is (A) zero, (B) low, (C) medium, and (D and E) high.

(F) Real and (G) imaginary parts of the propagating modes in the complex $\tilde{V}^2 - b$ space. The transformation $\frac{b}{|b|} log(1+|b|)$ is used to better visualize data. For the projections shown in the $\tilde{V}^2$ plane, no localized states exist in the gray region; orange region, only fundamental modes exist; pink region, fundamental modes and higher-order modes coexist; blue region, each fundamental mode bifurcates into two separate modes; the region beyond blue, bifurcated higher-order modes.

See also Figure S1.

$$-i\frac{\partial\phi}{\partial z}+\frac{1}{2k}\left(\frac{\partial^2}{\partial x^2}+\frac{\partial^2}{\partial y^2}\right)\phi+k_0(n-n_0)\phi=0 \qquad \text{(Equation 2)}$$

If we assume the field in the form $\phi = \psi(x,y)e^{-i\mu z}$, the equation can be further simplified to

$$\frac{1}{2k}\left(\frac{\partial^2}{\partial x^2}+\frac{\partial^2}{\partial y^2}\right)\psi+[k_0(n-n_0)-\mu]\psi=0 \qquad \text{(Equation 3)}$$

where μ is related to propagation constant β by the equation $\beta = k + \mu$.

Figures 2A–2E show the modal fields ψ in the cross section of a single-mode fiber when different amounts of gain are applied. A conventional single-mode optical fiber ($n_{I,1} = n_{I,2} = constant$) only supports the LP01 mode (Agrawal, 2007; Snyder and Love, 1983). As shown in Figure 2A, this mode has an intensity distribution that is similar to that of a Gaussian beam. Figure 2B shows the mode intensity profile with relatively low gain in the left section. In this case, the fiber still possesses a Gaussian-like distributed mode intensity, just like its conventional counterparts. If the gain keeps increasing, the mode intensity starts showing asymmetry with more energy residing in the doped section, as displayed in Figure 2C. As the gain coefficient g increases and exceeds a critical value, the fundamental mode will be confined in the left section (Figure 2D). Also, one can find that another new mode appears in the undoped section (Figure 2E).

The physics behind this phenomenon can be explained by noting the imaginary parts of the refractive index imposing on ψ. Both real and imaginary refractive indices can create optical potentials confining light field. When the amount of gain is small, light can be freely exchanged between core sections; hence the mode field distribution in the core is just like conventional fibers. With the increasing gain gradually creating stronger imaginary potentials, the energy flow between two sections begins to be reduced and light field starts to be trapped in the two potentials. As the imaginary potential strength increases beyond the threshold, the weaker energy flow is no longer able to sustain the integrity of the field, and, as such, the fundamental mode becomes two isolated modes in each site.

To give a broader insight into the modes supported by the fibers with asymmetric gain, we further present an analysis in the complex $\tilde{V}^2 - b$ space, where mathematical transformations are taken to make the results independent of particular fiber parameters. These transformations will not change the system's action. If we define a contrast factor $\Delta n_I = (n_{I,1} - n_{I,2})/2$, gauge transformation can be established by $\phi = \phi' \exp[-k_0(n_{I,1} - \Delta n_I)z]$ or $\phi' \exp\left[-k_0(\Delta n_I + n_{I,2})z\right]$. The real and imaginary parts of the complex-valued index are expressed in the dimensionless forms (Siegman, 2003, 2007).

$$\Delta n = \left(\frac{2\pi a}{\lambda}\right)^2 2 n_0 n_R \quad \text{(Equation 4)}$$

$$\Delta \alpha = \left(\frac{2\pi a}{\lambda}\right)^2 2 n_0 \Delta n_I \quad \text{(Equation 5)}$$

where a is the radius of the fiber core. With these definitions the conventional fiber V parameter takes on the complex-valued form

$$\tilde{V}^2 = \Delta n + i\Delta\alpha \quad \text{(Equation 6)}$$

The normalized propagation constant b is defined as (Gloge, 1971)

$$b = \frac{n_{eff}^2 - n_0^2}{(n_0 + n_R)^2 - n_0^2} \simeq \frac{n_{eff} - n_0}{n_R} \quad \text{(Equation 7)}$$

where n_{eff} is the effective index of each mode in the fiber.

Figures 2F and 2G plot the propagation regions and boundaries for the LP01 and LP11 modes in the complex $\tilde{V}^2 - b$ space. With the presence of increasing asymmetric gain, the modes lose their circular symmetry. When $\Delta\alpha$ goes beyond a critical value, the propagation constants bifurcate into a complex conjugated pair. This behavior is related to the parity-time phase transition in coupled waveguide system (Guo et al., 2009) (see Figure S1 for further details). To achieve good mode quality, currently almost all fibers employ circular symmetric or at least rotational symmetric refractive index profiles. Remarkably, Figures 2F and 2G also indicate the existence of a nontrivial regime, where $\Delta\alpha \ll \Delta n$ ($\Delta\alpha/\Delta n$ smaller than roughly 10^{-2} level). As a crossover from exact symmetry to strong asymmetry, the fibers in this regime, though having asymmetric gain, admit confined modes, which are almost the same as conventional fibers. Hence, their circular symmetry of the wave functions can be approximately preserved. This feature gives us a new degree of freedom with which we can tailor the gain spectra of fibers.

Therefore, we propose a single mode-fiber whose core incorporates two gain materials. Such fiber combines the gain spectra of different laser media, whereas its modal profile maintains circular symmetry. A model based on the rate equations is used to evaluate the performance of this new fiber (see Transparent Methods). Simulation results confirm our anticipation that gain bandwidth can be significantly extended (see Figures S2–S4).

On the basis of the theoretical analysis, we demonstrated a proof-of-concept fiber combining the spectra of thulium (Tm) and holmium (Ho) together. To fabricate a core with multiple sections, the fiber preform was made by the rod-in-tube technique (Figure 3A) rather than by the conventional MCVD method, by which gases are deposited on an axially rotated silica tube. Therefore, it would be very difficult, if not impossible, for the MCVD method to form an asymmetric structure. Another important advantage of the rod-in-tube method is that it supports multi-component silicate glasses, which allows access to high rare-earth-doping concentration and precise and independent control of refractive indices of the core and cladding (Lee et al., 2015). To simplify pump scheme, Tm ions were added to the Ho-doped glass. In this way, both sections can be excited by the same pump source at ~793 nm. Note that for the Tm-Ho codoped glass, Tm is not the active ion but a kind of sensitizer, which transfers energy to the activator. Thus the emission spectrum of Tm-Ho codoped glass cannot fully cover the range of Tm singly doped glass. The detail of the manufacturing process is provided in Transparent Methods.

An image of the cleaved fiber facet is shown in Figure 3B. The fiber has a double-clad structure with a 150-μm outer polymer cladding, a 110-μm inner cladding with a numerical aperture (NA) of ~0.6, and a 8.5-μm circular core with a NA of 0.14, which allows single-mode operation at wavelengths above ~1.6 μm. The loss is measured to be 5 dB/m at 2,097 nm. It is known that Tm generates emission centered at ~1.9 μm and Ho at ~2.1 μm. By doping one section of the bisected core with Tm ions and the other with Ho ions, two gain spectra from two sections are shared within the core, so a broadband amplified spontaneous emission (ASE) can be generated. As shown in Figure 3C, the ASE spectrum of 0.9 m proposed fiber exhibits a 3-dB bandwidth of ~160 nm, which, to the best of our knowledge, is the broadest ASE bandwidth directly from a gain fiber. By using the identical experimental setup, the ASE spectra from regular Tm-doped and Tm-Ho-codoped silicate fibers have a bandwidth of only ~90 and ~60 nm, respectively (Figures 3D and 3E).

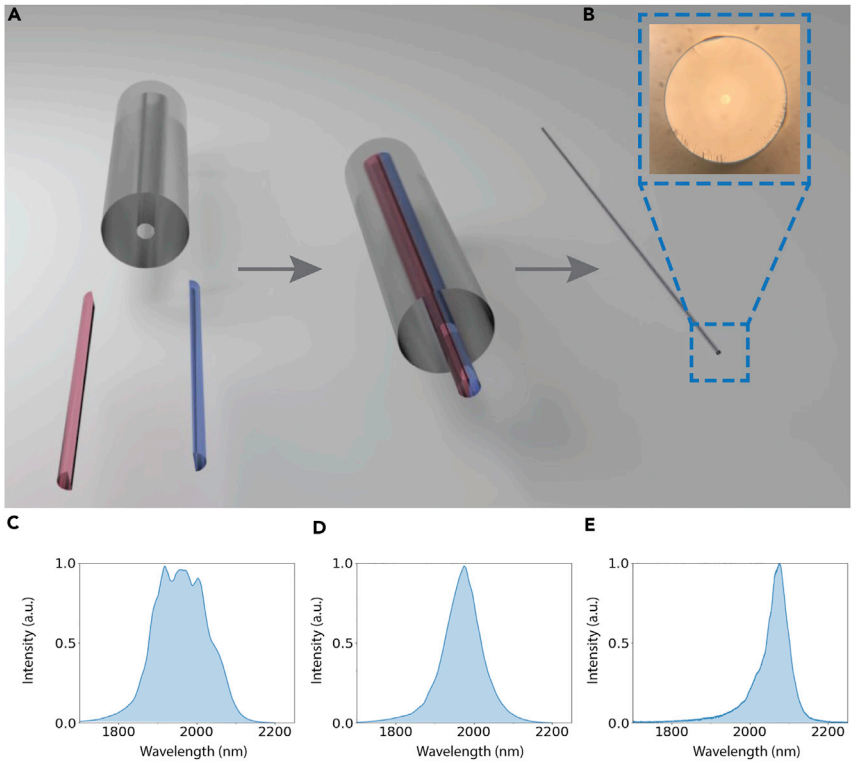

Figure 3. Fabrication and Characterization of Multi-section Core Fiber

(A) Schematic diagram of the rod-in-tube technique.

(B) The optical image of the fiber facet.

(C–E) The ASE spectrum from (C) proposed fiber, (D) Tm-doped fiber, and (E) Tm-Ho-codoped fiber.

To examine the mode quality, we built a laser amplifier comprising the proposed fiber, as shown in Figure 4A. Two seed lasers at 1,940 nm and 2,050 nm were used, respectively. Figure 4B shows the measurement of the output beam profiles at 1,940 and 2,050 nm. The Gaussian-like shape profile further confirms the single-mode feature predicted by the simulation. Therefore the introduction of asymmetric imaginary index does not compromise the transverse mode profile but enables the fabrication of fibers with better performance.

Besides significant extension of gain bandwidth, this fiber also opens up new possibilities for dual-wavelength lasers that can generate two widely separated wavelengths. Because a dual-wavelength laser can serve dual purposes with one single device, it is more cost effective and versatile when compared with lasers, which normally produce one single wavelength or two closely spaced wavelengths (Walsh, 2010). Dual-wavelength laser oscillators or amplifiers could be essential ingredients in many useful applications, such as remote sensing, optical communication, laser ranging, medical imaging, and spectroscopy (Walsh, 2010; Zhao et al., 2016; Xu and Wise, 2013), where multiple wavelengths are required for one device in a limited space. Therefore, compact dual-wavelength lasers are highly demanded.

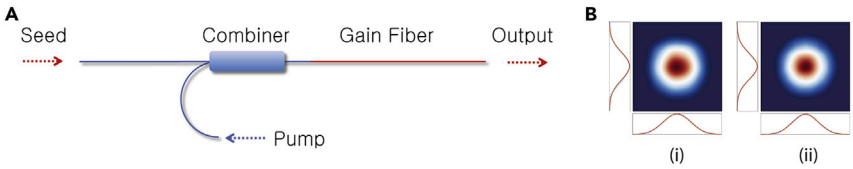

Figure 4. Mode Quality Examination

(A) Schematic of experimental setup.

(B) The output beam profiles at (i) 1,940 and (ii) 2,050 nm.

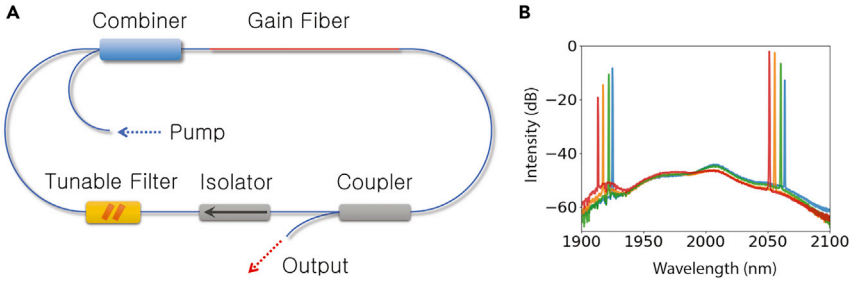

Figure 5. All-Fiber Tunable Dual-Wavelength Laser

(A) Schematic of the dual-wavelength fiber laser.

(B) Spectra of the dual-wavelength laser.

We went further by constructing an all-fiber tunable dual-wavelength laser with the proposed fiber, as illustrated in the Figure 5A. Figure 5B shows the output spectra, where two laser wavelengths can be found simultaneously with one ranging from 1,912 to 1,927 nm and the other ranging from 2,049 to 2,064 nm. The tunable range is as large as 15 nm. The total output power varies from 10 to 21 mW as wavelengths change. To further confirm that the dual-wavelength operation was the contribution of the multi-section core fiber, it was replaced by regular Tm-doped and Tm-Ho-codoped silicate fibers with only one core section, whereas the other components and parameters remained the same. Owing to strong gain competition among limited excited Tm or Ho ions, only one wavelength was obtained. It should be noted that dual wavelength from conventional fibers is achievable if the cavity reflectivities are carefully adjusted to balance the ion transition of each wavelength. However, such balance is so delicate that it will be broken easily once the pump power or ambient temperature is changed. In addition, those dual-wavelength lasers have small wavelength separations and their output wavelengths are fixed. Our work offers a way to develop compact dual-wavelength lasers with high stability and wide tunability. It is an important step toward the realization of multi-wavelength and multi-functional fiber lasers.

Although the above proof-of-concept fiber is based on Tm and Tm-Ho, this configuration can be extended to other rare earth combinations, such as Tm/Er, Er/Yb, and Yb/Nd. Further extension of emission wavebands can be achieved by including more core sections that are made of different rare earth dopants or host glasses. Simulations show that these fibers still possess a Gaussian-like transverse mode profile as displayed in Figure 6. In addition, this fiber configuration is compatible with other fiber designs. For example, one can introduce the multi-section core to photonic crystal fibers (Russell, 2003), which currently manipulate light flow through the microstructures in their cladding, and may open an avenue to versatile fibers with more intriguing properties.

In conclusion, we have presented a detailed theoretical study of the fiber with asymmetric gain profile and extended fiber mode theory to the complex space. Based on the analysis, we have proposed a new fiber configuration and experimentally demonstrated a multi-section core fiber with unique manufacturing strategy. Such fiber provides an effective approach of producing optical gain beyond that of a single laser material and should lead to breakthroughs in fiber light sources having broader bandwidth, shorter pulse width, and wider tunability.

Limitations of the Study

The all-fiber dual-wavelength laser showed relatively low output power. As the main purpose was to demonstrate stable and tunable dual-wavelength operation, no effort was made to optimize the output

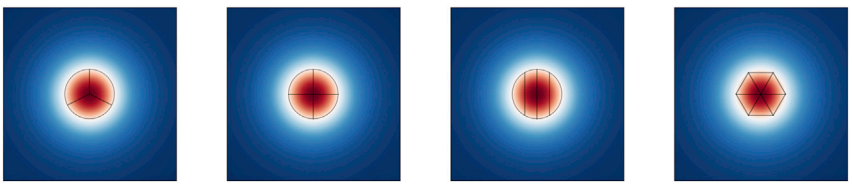

Figure 6. Several Examples of the Fibers with More Core Sections

power in this experiment. We believe that the low power was caused by the relatively high losses of some intracavity components (tunable filter and isolator) and a large improvement can be obtained by reducing these losses.

METHODS

All methods can be found in the accompanying Transparent Methods supplemental file.

SUPPLEMENTAL INFORMATION

Supplemental Information can be found online at https://doi.org/10.1016/j.isci.2019.11.017.

AUTHOR CONTRIBUTIONS

C.H. conducted the simulations and the experiments. T.L. fabricated the fibers. C.H. and J.H. performed the data visualization and analysis. All authors discussed the results. C.H., J.G., S.F., and S.J. wrote the manuscript with contributions from all authors. S.J. supervised the research.

DECLARATION OF INTERESTS

The authors declare no competing interests.

Received: July 4, 2019
Revised: September 25, 2019
Accepted: November 9, 2019
Published: December 20, 2019

REFERENCES

Agrawal, G.P. (2007). Nonlinear Fiber Optics (Academic Press).

Bookey, H.T., Lousteau, J., Jha, A., Gayraud, N., Thomson, R.R., Psaila, N.D., Li, H., MacPherson, W.N., Barton, J.S., and Kar, A.K. (2007). Multiple rare earth emissions in a multicore tellurite fiber with a single pump wavelength. Opt. Express *15*, 17554–17561.

Chong, A., Liu, H., Nie, B., Bale, B.G., Wabnitz, S., Renninger, W.H., Dantus, M., and Wise, F.W. (2012). Pulse generation without gain bandwidth limitation in a laser with self-similar evolution. Opt. Express *20*, 14213–14220.

Digonnet, M.J. (2001). Rare-Earth-Doped Fiber Lasers and Amplifiers, Revised and Expanded (CRC Press).

Fan, F., Turkdogan, S., Liu, Z., Shelhammer, D., and Ning, C. (2015). A monolithic white laser. Nat. Nanotechnol. *10*, 796.

Geng, J., and Jiang, S. (2014). Fiber lasers: the 2 mm market heats up. Opt. Photon. News *25*, 34–41.

Geng, J., Wang, Q., Lee, Y., and Jiang, S. (2014). Development of eye-safe fiber lasers near 2 μm. IEEE J. Sel. Top. Quantum Electron. *20*, 150–160.

Gloge, D. (1971). Weakly guiding fibers. Appl. Opt. *10*, 2252–2258.

Gmachl, C., Sivco, D.L., Colombelli, R., Capasso, F., and Cho, A.Y. (2002). Ultra-broadband semiconductor laser. Nature *415*, 883.

Guo, A., Salamo, G.J., Duchesne, D., Morandotti, R., Volatier-Ravat, M., Aimez, V., Siviloglou, G.A., and Christodoulides, D.N. (2009). Observation of p t-symmetry breaking in complex optical potentials. Phys. Rev. Lett. *103*, 093902.

Jackson, S.D. (2012). Towards high-power mid-infrared emission from a fibre laser. Nat. Photon. *6*, 423.

Koechner, W. (2006). Solid-State Laser Engineering (Springer Press).

Krauss, G., Lohss, S., Hanke, T., Sell, A., Eggert, S., Huber, R., and Leitenstorfer, A. (2010). Synthesis of a single cycle of light with compact erbium-doped fibre technology. Nat. Photon. *4*, 33.

Kucera, C., Kokuoz, B., Edmondson, D., Griese, D., Miller, M., James, A., Baker, W., and Ballato, J. (2009). Designer emission spectra through tailored energy transfer in nanoparticle-doped silica preforms. Opt. Lett. *34*, 2339–2341.

Di Labio, L., Lüthy, W., Romano, V., Sandoz, F., and Feurer, T. (2008). Superbroadband fluorescence fiber fabricated with granulated oxides. Opt. Lett. *33*, 1050–1052.

Lee, Y., Ling, H., Lin, Y., and Jiang, S. (2015). Heavily Tm^{3+}-doped silicate fiber with high gain per unit length. Opt. Mater. Express *5*, 549–557.

Li, T. (1985). Optical Fiber Communications: Fiber Fabrication (Academic Press).

Richardson, D.J. (2010). Filling the light pipe. Science *330*, 327–328.

Rösch, M., Scalari, G., Beck, M., and Faist, J. (2015). Octave spanning semiconductor laser. Nat. Photon. *9*, 42.

Russell, P. (2003). Photonic crystal fibers. Science *299*, 358–362.

Siegman, A. (2003). Propagating modes in gain-guided optical fibers. J. Opt. Soc. Am. A *20*, 1617–1628.

Siegman, A. (2007). Gain-guided, index-antiguided fiber lasers. J. Opt. Soc. Am. B *24*, 1677–1682.

Snyder, A.W., and Love, J.D. (1983). Optical Waveguide Theory (Chapman and Hall).

Walsh, B.M. (2010). Dual wavelength lasers. Laser Phys. *20*, 622–634.

Xu, C., and Wise, F.W. (2013). Recent advances in fibre lasers for nonlinear microscopy. Nat. Photon. *7*, 875–882.

Zhao, X., Hu, G., Zhao, B., Li, C., Pan, Y., Liu, Y., Yasui, T., and Zheng, Z. (2016). Picometer-resolution dual-comb spectroscopy with a free-running fiber laser. Opt. Express *24*, 21833–21845.

ISCI, Volume *22*

Supplemental Information

Rare Earth Doped Optical Fibers with Multi-section Core

Chongyuan Huang, Jihong Geng, Tao Luo, Jiali Han, Qing Wang, Rongguang Liang, Shanhui Fan, and Shibin Jiang

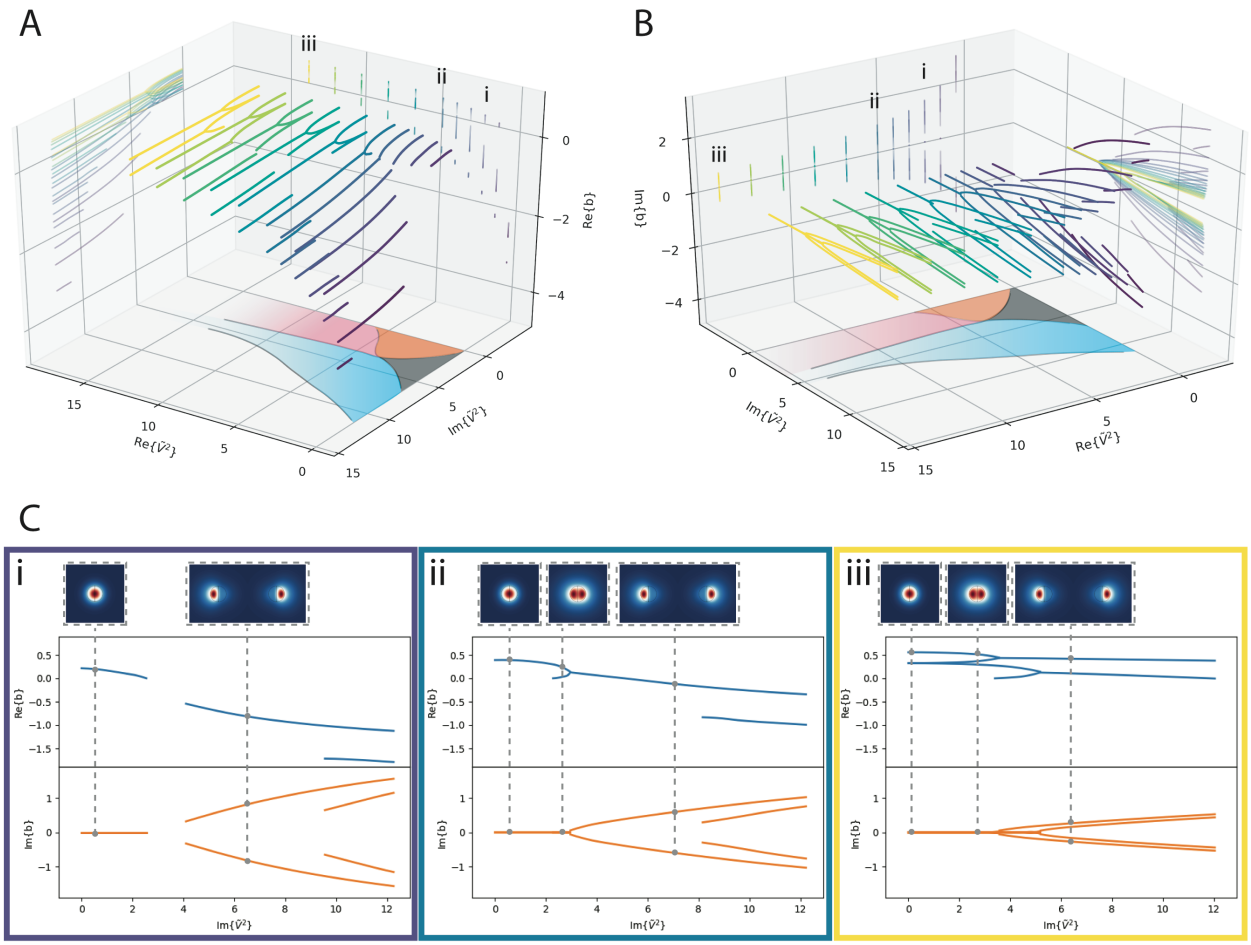

Figure S1. Supported mode propagation regions and boundaries. Related to Figure 2. (A) and (B) are real and imaginary part of *b* in the complex $\tilde{V}^2 - b$ space, respectively. For both conventional passive and active fibers whose gain coefficients are homogeneous over the core, their imaginary refractive indices become zero after gauge transformation. Therefore, their propagation modes occur along the positive real $\tilde{V}^2$ axis. The LP01 mode can be find everywhere, while LP11 mode appears when Δn is beyond ~5.8. (C) shows snapshots of *b* traces and beam profiles with different Δn as indicated in (A) and (B). For a fixed value of $\Delta n \lesssim 3.7$, as shown in (C i), the normalized propagation constant *b* of fundamental mode LP01 decreases when $\Delta\alpha$ (i.e. $Im\{\tilde{V}^2\}$) is increasing, and it disappears at the boundary of the gray region where no localized states exist. Below the boundary, the eigenvalues of the structure are completely real. If increasing $\Delta\alpha$ further to a large enough value, the waveguiding will be turned back on again, but the stronger imaginary potentials bifurcates the fundamental mode into two separate complex modes. (C ii) shows the case when $3.7 \lesssim \Delta n \lesssim 5.8$. One may find a second real propagation constant *b* at some values of $\Delta\alpha$. It actually is a branch of LP11 mode. With the increase of $\Delta\alpha$, the propagation constants of LP01 and LP11 modes approach each other, and finally merge into one at a critical point. Above this point, a pair of complex conjugate *b* emerges, corresponding to the mode pair shown in Figures 2D and 2E. Further increasing of Δn results in emerging of another branch of LP11 mode, which will be converted into a pair of complex conjugate propagation constants when the parameter $\Delta\alpha$ goes beyond the higher order threshold, as shown in (C iii). Considering the above behavior of modal fields and the configuration of the proposed fiber, it is worth to mention parity-time (PT) symmetry (see Bender et al., 1999; Bender, 2005; Feng et al., 2017; Longhi, 2017, and references therein). From a quantum mechanics perspective, parity (P) symmetry of the

system will be broken when the asymmetric gain is added. However, the proposed structure actually belongs to the family of another kind of symmetry, so called “PT symmetry”. For a PT symmetric structure, its associated Hamiltonian *H*, though becomes non-Hermitian, can still possess entirely real spectra below threshold. On the other hand, if this limit is crossed, the spectrum is no longer real, and imaginary eigenvalues emerge. This is the onset of PT-symmetry breaking. Inspired by its fascinating features, integrated optical devices based on spontaneous PT symmetry breaking have been theoretically proposed or experimentally fabricated (Feng et al., 2017; Longhi, 2017). Different from previous theoretical simulations or experimental demonstrations, the proposed fiber is a coupled system combining two PT symmetric structures together (one wavelength’s gain area is the other’s loss). Additionally, to keep a Gaussian-like mode profile, the fiber works in the unbroken PT symmetry phase, where the non-Hermitian system has entirely real eigenvalues and symmetric eigenfunctions.

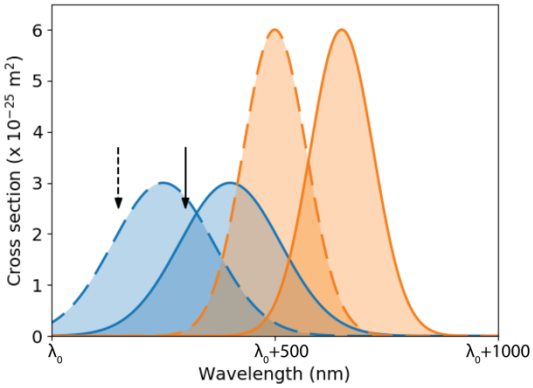

Figure S2. Absorption (blue) and emission (orange) cross sections of Ion 1 (dash) and Ion 2 (solid). Related to Figure 1 and 2.

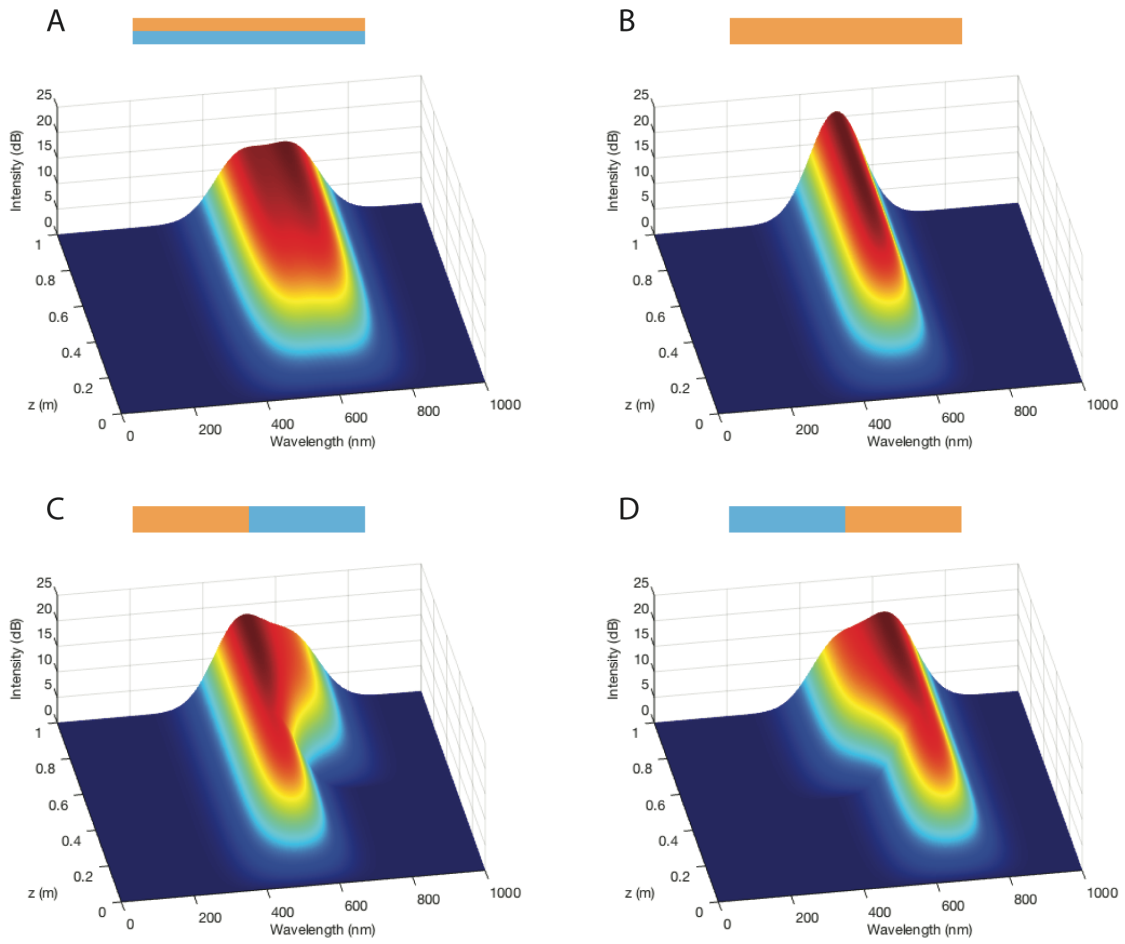

Figure S3. Output spectra of the ideal case where there is no signal reabsorption. Related to Figure 1 and 2. (A) shows the proposed fiber with each section doped with Ion 1 or Ion 2. Compared with conventional single core section fiber shown in (B), the output spectrum from the proposed fiber has a much broader 3-dB bandwidth, improving from 81 nm to 216 nm, which is the combination of emission spectra from two kinds of active ions. Apparently, combining emission of two dopants can also achieved by simply splicing two kinds of conventional fibers together. However, signal light will experience discrete gain when it propagates through the longitudinally connected fibers. As shown in (C), the shorter wavelength part of the signal spectrum was amplified in the first half of the concatenated fiber, and then the longer wavelength part in the second half. Although a 152 nm bandwidth spectrum could be generated from the output end, the signal is still suffering from the gain-bandwidth limitation in each half of the concatenated fiber. Similar scenario can be observed in (D), where the positions of two fibers are exchanged with each other. On the other hand, every cross section of the proposed fiber contains two kinds of ions and thus provides gain for every wavelength within the emission spectra of these ions, thereby effectively extending the bandwidth. This combined gain, longitudinally distributed along the fiber, can prevent the signal power at either longer (the case in C) or shorter (the case in D) wavelengths from dropping too low during the propagation inside fiber. This is essential for the applications like optical communication, since excessive noise will be introduced when signal power is close to the noise floor. Note that the peak gain is decreased from ~18 dB to ~15 dB by changing from conventional fibers to the multi-section core fiber. This reduction is mainly caused by energy conversation and can be compensated by using stronger pump excitation and/or higher doping concentration.

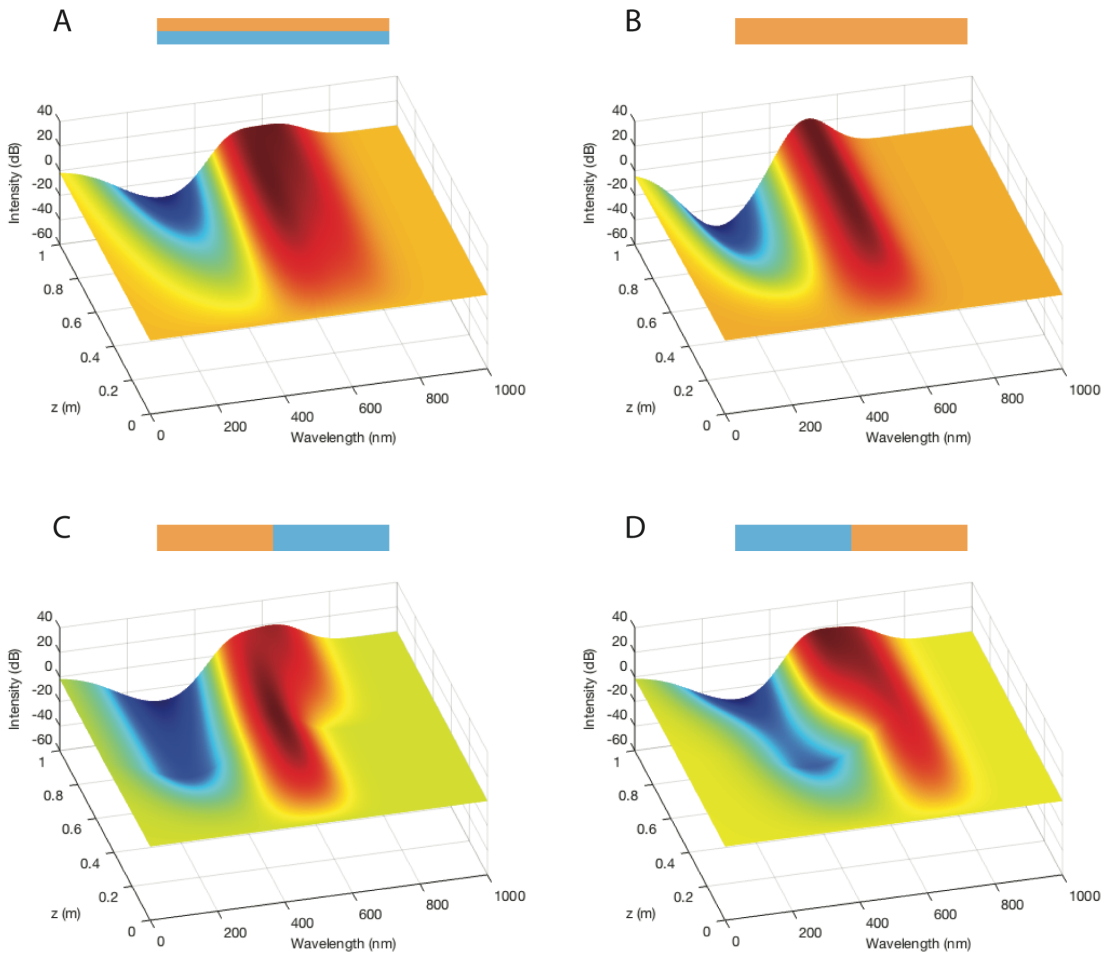

Figure S4. Output spectra from different fibers with reabsorption effect. Related to Figure 1 and 2. (A) Proposed fiber with each section doped with Ion 1 or Ion 2. (B) single fiber doped with Ion 1. (C) Ion 1 doped fiber followed by Ion 2 doped fiber. (D) Ion 2 doped fiber followed by Ion 1 doped fiber. The result is similar to the case shown in Figure S3. Because of the presence of two different emission and absorption cross sections, the gain spectra with tailored shape should be achievable by adjust doping concentrations.

Transparent Methods

Fiber Spectra Simulation

A numerical model based on the rate equations is used to evaluate the performance of the proposed fiber configuration. The simulation does not attempt to reproduce the exact results, instead, it focuses on qualitative prediction and illustrates the idea of "spectra tailoring" through a special core design. For simplicity, and without loss of generality, two level systems are considered here. If the population density of each energy level is N_x (x = 1, 2), with cross section σ_{mn} and relaxation time τ_{mn} representing the energy transfer process from the m-th level to the n-th level, the rate equations for local upper and lower energy levels of each section are given by (Paschotta et al., 1997; Jackson and King, 1999; Eichhorn, 2005)

$$\frac{dN_2^i}{dt} = W_{p12}^i N_1^i - W_{p21}^i N_2^i - \frac{N_2^i}{\tau_{21}^i} - W_{s21}^i N_2^i + W_{s12}^i N_1^i \tag{S1}$$

$$\frac{dN_1^i}{dt} = -W_{p12}^i N_1^i + W_{p21}^i N_2^i + \frac{N_2^i}{\tau_{21}^i} + W_{s21}^i N_2^i - W_{s12}^i N_1^i \tag{S2}$$

$$N^i = N_1^i + N_2^i \tag{S3}$$

where *i* corresponds to Section 1 or 2. The transition rates related to pump and signal wavelengths are

$$W_{p12}^i = \sigma_{p12}^i \frac{\Gamma_p^i P_p^i \lambda_p^i}{hcA} \tag{S4}$$

$$W_{p21}^i = \sigma_{p21}^i \frac{\Gamma_p^i P_p^i \lambda_p^i}{hcA} \tag{S5}$$

$$W_{s12}^i = \sum_j \sigma_{p12}^{i,j} \frac{\Gamma_s^j P_s^j \lambda_s^j}{hcA} \tag{S6}$$

$$W_{s21}^i = \sum_j \sigma_{p21}^{i,j} \frac{\Gamma_s^j P_s^j \lambda_s^j}{hcA} \tag{S7}$$

here *h* is the Planck constant; *A* is the area of beam cross section, which approximately equivalent to fiber core; and P_p (P_s) and λ_p (λ_s) are the total power and central wavelength of the pump (signal) light, respectively. The overlap factors Γ_p and Γ_s are introduced since each core section is doped with one kind of active ions and only interact with some fraction of the pump and signal powers over the cross section.

For the steady state, the population densities of each level are written as

$$N_2^i = \frac{W_{p12}^i + W_{s12}^i}{W_{p12}^i + W_{s12}^i + 1/\tau_{21}^i + W_{p21}^i + W_{s21}^i} \tag{S8}$$

$$N_1^i = N^i - N_2^i \tag{S9}$$

The forward and backward beam propagation and amplification in the fiber are governed by

$$\frac{dP_p^{\pm,i}}{dz} = \mp[\Gamma_p^i(\sigma_{p12}^i N_1^i - \sigma_{p21}^i N_2^i) + \delta_p]P_p^{\pm,i} \tag{S10}$$

$$\frac{dP_s^{\pm,j}}{dz} = \sum_i \pm[\Gamma_s^{i,j}(\sigma_{s21}^{i,j} N_2^i - \sigma_{s12}^{i,j} N_1^i) + \delta_s^j]P_s^{\pm,j} \pm \Gamma_s^{i,j}\sigma_{s21}^{i,j} N_2^i \frac{2hc^2}{(\lambda_s^j)^3} \tag{S11}$$

These equations can be solved numerically by the Runge-Kutta method. For illustration purpose, some typical parameter values were adopted in the simulation. We assume the absorption and emission cross

sections of two different ions have Gaussian lineshape and plotted in Figure S2. The pump wavelength for different core sections are indicated by black arrows. The lifetime τ_{21} is ~300 μs and fiber length is 1 m with a core diameter of 10 μm. Doping concentration of both sections is $5 \times 10^{25}\ m^{-3}$. The input signal has a uniform power of 0.1 mW at each wavelength channel from λ_0 nm to $\lambda_0 + 1000$ nm. Although the above simulation is based on two level systems, it can be easily adapted to more complex and accurate models by incorporating additional equations. For instance, thulium-doped fiber laser pumped by ~793 nm is a four-level system with cross-relaxation process, while the thulium-holmium-codoped fiber laser pumped by ~793 nm has a four-level and a two-level system with energy transfer process between them. When they are employed to comprise a multi-section core fiber, the model can be built by simply replacing the Eqs. S1-S3 with the corresponding rate equations which have been widely used in modeling rare-earth doped fiber lasers (Paschotta et al., 1997; Jackson and King, 1999; Eichhorn, 2005; Barnes et al., 1996; Jackson, 2006).

Fiber Fabrication

The fiber preform is based on AdValue Photonics' multi-component silicate glasses (SG4x, SGC32), which include SiO_2, Al_2O_3, BaO, ZnO, and La_2O_3. The adding of Al_2O_3 can enhance mechanical strength and chemical durability. One core glass is doped with 5 wt% Tm ions and the other is codoped with 6 wt% Tm ions and 0.8 wt% Ho ions. The refractive index of both doped glasses is matching with each other. These glasses have compatible chemical and thermomechanical characteristics, especially their softening temperature and thermal expansion coefficient. Therefore, they are good candidates for fabricating the proposed fiber. In order to produce the multi-section core, the bulk core glasses were carefully polished and ground until they form semi-cylindrical rods. When the grounded surfaces were disposed in contact with one another, the resultant two semi-cylindrical rods formed a cylinder. The cylindrical rod made of Tm-doped glass and Tm-Ho-codoped glass was inserted into the cladding glass tube to form the preform, as shown in Figure 3A. Both inside and outside surfaces of the glass tube were polished, and its inner diameter was matched to the diameter of core rod. The completed preform was then placed into a fiber drawing tower and drawn into fibers. An argon gas atmosphere was applied to reduce absorption of water in the air. During the fiber drawing process, the two core glasses were physically bonded to form the single mode core.

Fiber Testing

The mode profiles were measured from a laser amplifier comprising the multi-section-core fiber, a pump combiner, and a laser diode, as shown in Figure 4A. The wavelengths of the seed lasers were centered at 1940 nm and 2050 nm, respectively. A long pass filter was used to eliminate the pump from the signal.

The all-fiber tunable dual-wavelength laser was constructed with the multi-section-core fiber, as illustrated in the Figure 5A. A laser diode at 793 nm was used to pump a 0.9 m multi-section-core fiber via a combiner. The broad wavelength tunability was achieved by using a fiber Fabry-Perot tunable filter (FFP-TF), which has a free spectral range (FSR) of ~159 nm, an insertion loss of ~1.5 dB, and a finesse of ~2300. The laser wavelength was determined by the transmission wavelength of the Fabry-Perot cavity, which in turn was piezoelectrically controlled by the voltage applied to the filter.

References

Barnes, N. P., Filer, E. D., Morrison, C. A., and Lee, C. J. (1996). Ho Tm Lasers I: Theoretical. IEEE J. Quantum Electron., 32, 92-103.

Bender, C. M., Böttcher, S., and Meisinger, P. N. (1999). PT-symmetric quantum mechanics. J. Math. Phys. 40, 2201-2229.

Bender, C. M. (2005). Introduction to PT-symmetric quantum theory. Contemporary Physics 46, 277-292.

Eichhorn, M. (2005). Numerical modeling of Tm-doped double-clad fluoride fiber amplifiers. IEEE J. Quantum Electron. 41, 1574-1581.

Feng, L., El-Ganainy, R., and Ge, L. (2017). Non-Hermitian photonics based on parity-time symmetry. Nature Photonics 11, 752-762.

Jackson, S. D., and King, T. A. (1999). Theoretical model of Tm-doped silica fiber laser. J. Lightw. Technol. 17, 948-956.

Jackson, S. D. (2006). Midinfrared Holmium Fiber Lasers. IEEE J. Quantum Electron. 42, 187-191.

Longhi, S. (2017). Parity-time symmetry meets photonics: A new twist in non-Hermitian optics. EPL 120, 64001.

Paschotta, R., Nilsson, J., Tropper, A. C., and Hanna, D. C. (1997). Ytterbium-doped fiber amplifiers. IEEE J Quantum Electron. 33, 1049-1056.